Dual-channel sensing strategy based on gold nanoparticles cooperating with carbon dots and hairpin structure for assaying RNA and DNA

Dan Zhong, Kuncheng Yang, Yingyi Wang, Xiaoming Yang

www.elsevier.com/locate/talanta

PII: S0039-9140(17)30756-7
DOI: http://dx.doi.org/10.1016/j.talanta.2017.07.035
Reference: TAL17734

To appear in: *Talanta*

Received date: 11 May 2017
Revised date: 8 July 2017
Accepted date: 13 July 2017

Cite this article as: Dan Zhong, Kuncheng Yang, Yingyi Wang and Xiaoming Yang, Dual-channel sensing strategy based on gold nanoparticles cooperating with carbon dots and hairpin structure for assaying RNA and DNA, *Talanta* http://dx.doi.org/10.1016/j.talanta.2017.07.035

Dual-channel sensing strategy based on gold nanoparticles cooperating with carbon dots and hairpin structure for assaying RNA and DNA

Dan Zhong, Kuncheng Yang, Yingyi Wang, Xiaoming Yang*

College of Pharmaceutical Sciences, State Key Laboratory of Silkworm Genome Biology, Southwest University, Chongqing 400715, China

*Correspondence to: Tel.: 86 23 68251225; fax: 86 23 68251225. ming4444@swu.edu.cn

Abstract

By employing the attractive performance of fluorescent carbon dots and the assistant of hairpin structure, an innovative dual-channel biosensor on the basis of gold nanoparticles (AuNPs) for detecting multiple nucleotide sequences has been successfully proposed. In brief, the fluorescence of carbon dots (CDs) was quenched in the absence of the targets, and the hairpin structure was hybridized with the AuNPs-DNA and resulted in recovering the fluorescence. Instead, the presence of breast cancer (BRCA1) RNA/DNA could specifically bind with its contrary sequence to release the CDs from AuNPs, hence leading to the fluorescence recovery as a positive signal. Again, the hairpin structure can be released in the presence of thymidine kinase (TK1) RNA/DNA, thus induced a fluorescence quenching accordingly. Subsequently, the prepared sensing model was applied to detect BRCA1 RNA/DNA respectively accompanied with a linear range of 4-120 nM as well as a detection limit of 1.5 nM and 2.1 nM, and 10 nM-120 nM as well as a detection limit of 3.6 nM and 4.5 nM for TK1 RNA/DNA respectively. More importantly, this sensing model could assay any possible gene sequence or aptamer-substrate

complexes by appropriately programming.

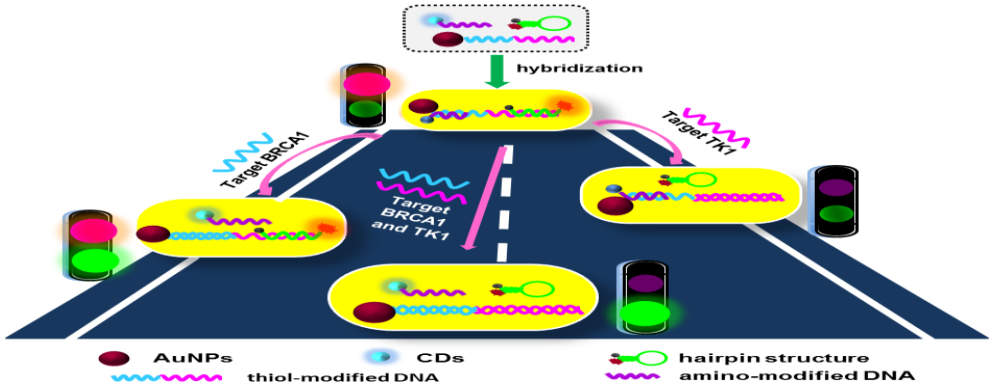

By employing the attractive performance of fluorescent carbon dots and the assistant of hairpin structure, an innovative dual-channel biosensor on the basis of gold nanoparticles (AuNPs) for detecting multiple nucleotide sequences has been successfully proposed. More importantly, this sensing model could assay any possible gene sequence or aptamer-substrate complexes by appropriately programming.

Keywords: Carbon dots; Gold nanoparticles; Hairpin structure; Assaying; Nucleic acid

Introduction

Nucleic acid detections, especially DNA and RNA analysis, mainly associated with medical diagnostics and disease pathophysiology are meaningful, since the human genome sequences and their related functions play a critical role in the biological and medical fields [1-3]. Several methods for RNA detection mainly including reverse transcription-polymerase chain reaction (RT-PCR), Northern

blotting, in situ hybridization, solid-phase assays, and microarrays have been developed, belonging to the elaborate multi-step methods. Furthermore, the similar defects of requiring highly skilled operators and expensive instrumentation and time consuming also limited their applications. For both the elucidation of gene expression patterns in biological systems and early identifying cancer and other diseases, therefore, more creative methods for the rapidly simultaneous and quantitative detection of multiple RNA at are still being actively pursued [4].

CDs are fascinating carbon materials owing to their unique properties consisting of stable photoluminescence, tunable excitation and emission wavelength, lack of optical blinking, small size, low toxicity and favorable biocompatibility [5-7]. Thereby, this kind of material has drawn considerable attentions in the fields of nanobiotechnology, biological labeling [8], photocatalysis, sensing, biomedicine and delivering drugs [9-11]. During the past few years, two major approaches have been raised for synthesizing CDs. One way was known as the top down, consisting of electrochemical oxidation, acidic oxidation, arc discharge and laser ablation. For the other way, hydrothermal, microwave and ultrasonic defined as the bottom up, have been generally applied to synthesize CDs [12-14]. Compared with conventional organic dyes and semiconductor quantum dots (QDs) that are seriously pernicious for human health and the environment, CDs exhibited fascinating properties and potentiality not only in theoretical but also in practical aspects. Especially, numerous CDs have been utilized to design fluorescent probes towards various purposes [15-18].

Since the single-stranded DNA (ssDNA)-derivatized AuNPs was first reported by the Mirkin group in 1997, numerous efforts have been devoted to intensively explore this type of new biosensor over the past two decades [19]. Basically, this conjugates show highly attractive properties including low/noncytotoxicity, biocompatibility, good stability in high salt biological buffers, improved resistance against nuclease degradation, and universally high cell uptake via scavenger receptor-mediated endocytosis pathways [20]. Hence, they were demonstrated as building blocks for nanotechnology, biosensing, materials science, and medicine [21-23]. In general, most applications of DNA-AuNPs employ the chemisorption of thiol-modified oligonucleotides onto the surfaces of these particles [24]. Moreover, AuNPs can serve as the ultra-efficient quenchers of molecular excitation energy while the fluorophore is placed in a close proximity ($<$ 5 nm) to the nanostructured metal surface [25], which is associated with their large ratio of the surface area versus volume and easy surface functionalization [26]. Thus, it has opened new perspectives to detect biomolecules by using fluorescence resonance energy transfer (FRET) with high sensitivity, owing to their broad absorption spectrum within the visible light range that overlaps with the emission wavelengths of the common energy donors [27]. Importantly, there existed reports for the fluorescence energy transfer from CDs to AuNPs once these two were brought into a close proximity, leading to FRET occurring [26].

Hereby, AuNPs about 13 nm in diameter were chosen because they can be readily prepared with little deviation in size and exhibit a sharp plasmon absorption band

(maximum absorbance at wavelength 520 nm) [19]. Inspiring by the valuable functions of AuNP-loaded ssDNAs and the attractive fluorescent performance of CDs, a novel dual-channel biosensor on the basis of CDs and AuNPs as the energy donor-receptor pairs together with hairpin structure (a fluorescent dye of cy3 at 5' end and a fluorescence quencher BHQ2 at 3' end) built up. Subsequently, this sensor was employed for sensitively and accurately detecting nucleic acid multiplexed. To be specific, the capture probe was initially designed by AuNPs-loaded thiol-modified ssDNA (AuNPs-DNA) composed by the corresponding sequences, recognizing and complementing the target genes associated with the breast cancer (BRCA1 RNA/DNA) and the thymidine kinase (TK1 RNA/DNA) genes. Meanwhile, both CDs conjugating with amine-modified DNA (CDs-DNA) and hairpin structure (HS) play the roles as the fluorescent signals. At the beginning, CDs-DNA and AuNPs-DNA complemented with each other in the absence of the targets, forming a close proximity between CDs and AuNPs, and the fluorescence of CDs was accordingly quenched. Similarly, the HS hybridized with the AuNPs-DNA and resulted in recovering the fluorescence of cy3. On the contrary, while BRCA1 RNA/DNA exists, it can specifically bind with AuNPs-DNA and replace the CDs from AuNPs, inducing the fluorescence recovery as a positive signal. In the same way, HS can be released and quenching the fluorescence of cy3 in the presence of TK1 DNA/RNA (Scheme 1).

More meaningfully, this designed approach allows the multiple analyses of nucleic acid, and also for any gene or aptamer-substrate complexes by appropriately programming the current sensing model. Compared with the traditional methods, this

solution has proposed the dual-channel assaying strategy for nucleic acid. Also, it has largely shortened the detection time to less than 1 h and allowed the whole process with the scarce interference from the complex samples. Meaningfully, the proposed strategy by employing DNA modified CDs, AuNPs-DNA and hairpin structure for multiplexed analyzing of nucleic acid was raised for the first time.

2. Materials and Methods

2.1 Preparation of DNA loaded on AuNPs and CDs modified with DNA

For preparing AuNPs-DNA [28], 310 μL (10 μM) of thiol-modified oligonucleotides were added to 1 mL as prepared AuNPs and shaken overnight. After 16 hours, the phosphate buffer (0.1 M; pH 7.4) was introduced into to the mixture to achieve a 0.01 M phosphate concentration. Over another eight-hour period, aliquots of sodium chloride solution (2.0 M) were added to the above mixture for reaching a final sodium chloride concentration of 0.3 M. Keeping reacting for more 12 hours, the solution containing the functionalized particles was centrifuged (15000 rpm, 25 min) and re-suspended in 1 mL PBS buffer (20 mM phosphate with 0.3 M NaCl, pH 7.4) three times to produce the purified AuNPs-DNA, which were used in all subsequent experiments.

For preparing CDs-DNA, the CDs solution were first diluted to 0.24 mg/mL by MES buffer (20 mM, pH 5.0), then 4 mg of fresh EDC and NHS were successively introduced into 1 mL of the prepared CDs for activating the carboxyl groups on their surfaces, and followed by reacting with rotation for 4 h at room temperature. After that, the mixture was centrifuged (50000 rpm, 30 min) to remove the excess regents.

Then, the precipitate was dissolved in 1 mL PB buffer (20 mM, pH 7.4). Next, amino-modified oligonucleotides were dissolved in PBS (20 mM phosphate with 0.3 M NaCl, pH 7.4) to form a transparent solution (2 μM). And then, 1 mL of this DNA solution was introduced into the activated CD solution, and further gently stirred for 6 h at room temperature. At last, 5000 MWCO of dialysis membrane was applied to remove the unreacted CDs and DNA.

2.2 Quantitation of thiol-oligonucleotides loaded on AuNPs

The quantitation of thiol-oligonucleotides loaded on AuNPs was performed by following a previous report [29, 30]. Initially, dithiothreitol (DTT) was dissolved in PBS buffer to form a final concentration of 1 M. Then, 1 mL DTT solution was added to 1 mL AuNPs-DNA as prepared. After 16 h of intermittent shaking at room temperature, the surface-bound oligonucleotides were chemically dissociated form the AuNPs surface. Meanwhile, the color of AuNPs solution became black and AuNPs aggregated afterward. The solutions containing dissociated oligonucleotides were separated from AuNPs by centrifugation at 10000 rpm for 10 min. Then, equal volumes of the dissociated oligonucleotides and a series concentration of HS were mixed and incubated for 30 min. A standard calibration curve of HS was obtained at the same time using the thiol-oligonucleotides samples prepared with the same DTT buffer solution. Finally, the average number of oligonucleotides per AuNPs was calculated through dividing the measured oligonucleotide molar concentration by the original AuNPs concentration. Importantly, the environment conditions of the sample and calibration standard solutions were paid a close attention to keep the same for all

the measurements.

2.3 Optimization

Optimizing the amount of HS: To explore the activity of modified thiol-oligonucleotide for hybridization and optimize the concentration of HS added, equal volumes of the prepared AuNPs-DNA (100 μL) and varied concentrations of HS (100 μL) were mixed and incubated for 18 min to allow hybridization. Then, the unreacted HS were removed by centrifugation (15000 rpm, 25 min) and resuspened in 200 μL PBS. Finally, the fluorescence variation of cy3 was recorded by FL spectrometer.

Optimizing the amount of CDs-DNA: Similarly, 500 μL AuNPs-DNA as prepared was mixed with 500 μL CDs-DNA (0.12 mg/mL). After 18 min incubation, the mixture was centrifuged to separate the nonhybridized CDs-DNA. Meanwhile, the standard curve of CDs-DNA was prepared with certain concentrations of CDs-DNA in the same detection conditions. The amount of hybridized CDs-DNA was determined by the fluorescence intensity of CDs-DNA.

Taken the optimized conditions together, 1 mL HS (176 nM) and 1 mL CDs-DNA (70. 8 μg/mL) were suspended to 1 mL AuNPs-DNA to build up the sensing system and stored in the dark for 18 min to allow hybridization. Then, the solution was centrifuged (15000 rpm, 25 min) and resuspended in 3 mL PBS (20 mM phosphate with 0.3 M NaCl, pH 7.4). Finally, the analyses were performed in a reaction volume of 400 μL that included 200 μL of the sensing model, 100 μL PBS buffer, 50 μL TK1 DNA/RNA and 50 μL BRCA1 DNA/RNA. After incubated for 20 min, the

fluorescence variations of cy3 and CDs were subsequently recorded by FL spectrometer.

3. Results and discussion

3.1 Characterization of CDs and AuNPs

Basically, the CDs described here served as a foundation of the detection strategy, thus all the work started with characterizing this CDs. Firstly, the maximum excitation and emission spectra of CDs were recorded as 345 nm and 430 nm respectively (Fig. S1A), and their fluorescent properties were subsequently explored. To be specific, the CDs solution obviously emitted the blue fluorescence (photograph b) irradiated by a UV lamp (365 nm) while appeared slightly transparent under daylight (photograph a). Again, the UV-vis absorption spectrum showed a peak at 333 nm owing to n–π* transition of C=O (Fig. S2). The surface functional groups of the CDs were validated by Fourier Transform Infrared spectrometer (FTIR). As shown in Fig. S1B the absorption band appearing at 3412 cm^{-1} and 3213 cm^{-1} were assigned to stretching vibrations of O-H and N-H. Meanwhile, the absorption band appearing at 2358 cm^{-1} referring to the stretching vibrations of C≡C. Moreover, the band at 1662 cm^{-1} was related with the stretching vibrations of C=O or C=C, however, the UV-vis absorption spectrum (Fig. S2) displayed a peak at 333 nm originated from n–π* transition of C=O, indicating there was C=O only. The peaks in the range 1000-1400 cm^{-1} indicated the existence of O-H and C-O groups. Taken together, these data revealed there were O-H, N-H, C≡C, C=O and C-O groups on the surface of the current CDs. Considering these groups on CDs, amino-modified oligonucleotides can be modified

on the surfaces of CDs by -COOH and -NH_2, while EDC and NHS function as the crosslinking agents. For further investigation of the nanostructures of CDs and AuNPs, HR-TEM was employed to directly observe the morphology and particle size distributions (Fig. S1C and S1D), and the CDs and AuNPs were spherical and well-dispersed. For the size distribution analysis, the diameter of CDs and AuNPs were in the range of 4.3±1.5 nm and 13.3±2 nm respectively (Fig. S1C and S1D). All the above data claimed a successful synthesis of the functional CDs and AuNPs, providing their possibility for the further applications.

3.2 Characterization of AuNPs-DNA and CDs-DNA

Since the citrate-stabilized AuNPs commonly used are only dispersed stably in an aqueous solution with a low ionic strength, the presence of more than 50 mM NaCl may induce irreversible aggregations of the AuNPs (Fig. 1A photograph b) [29]. In striking contrast, the DNA-capped AuNPs were stable in aqueous solutions even in the presence of 0.3M NaCl (Fig. 1A photograph c). Meanwhile, the UV-vis absorption spectra described that the maximum absorption of the AuNPs was at 521 nm, but it shifted to 525 nm after conjugating with DNA as well as the color of AuNPs became heavier from wine red (Fig. 1A), confirming that the AuNPs were successfully functionalized with DNA strands. Assuming uncoated spherical particles, the concentration of AuNPs was 13.78 nM after calculation [31].

Furthermore, the amount of thiol-oligonucleotides modified on the AuNPs was also investigated following previous reports (Fig. 2A) [29, 30]. Specifically, all the oligonucleotides were dissociated from the AuNPs surface by using DTT to rapidly

displace the bonds between oligonucleotides and AuNPs via an exchange reaction, and the aggregated AuNPs were subsequently removed. HS as the fluorescence signal was added into the above solution, and the concentration of HS was accordingly associated with the released oligonucleotides, so that the fluorescence intensity of cy3 can be used to determine the amount of oligonucleotide released from AuNPs. Thereby, the standard calibration curve for the fluorescence intensity of cy3 as the amount of HS varying was obtained by using the thiol-oligonucleotides samples prepared with the same DTT buffer solution (Fig. S3A and S3B). As shown in Fig. 2B and 2C, the fluorescence intensity of cy3 varied along with different concentrations of HS, and it reached the maximum at 6560 arbitrary units (a.u.). This suggested that all of the released oligonucleotides hybridized with HS, resulting in the increase of the fluorescence intensity for cy3. And it can be converted to the molar concentration using the as-built standard curve. By the corresponding calculation, each AuNPs was modified with approximately 32.3 DNA strands, and its related concentration of the modified oligonucleotides on AuNPs-DNA was 444.5 nM, showing the agreement with that of a previous report [32].

Again, amino-modified oligonucleotide was then equipped on the surfaces of CDs through the condensation reaction of amine and carboxyl, while EDC and NHS played the roles as the crosslinking reagents. In brief, the fluorescence intensity of CDs-DNA showed a little increase and the maximum emission was slightly shifted to 435 nm compared with that of CDs themselves (Fig. 1B). Meanwhile, the FTIR spectrum of CDs-DNA (Fig. 1C) was employed for investigating their functional

groups. Compared with that of CDs (Fig. S1B), the characteristic absorption peaks of CDs appeared still, indicating that this modification brought scarce influence on CDs. Furthermore, the conjugated amount of amino-modified oligonucleotide with CDs was further optimized by agarose gel electrophoresis (Fig. 1D). The gradual reduction of the band width of the amino-modified oligonucleotide in pace with increasing concentration of introduced CDs demonstrated the optimized amount of CDs to obtain CDs-DNA was 0.12 mg/mL. Based on the region of interest (ROI) analysis by the electrophoresis, the conjugation efficiency between 0.24 mg/mL of the CDs and 2 μM of the amino-modified oligonucleotide was 48%.

3.3 Building up the dual-channel sensing model

Towards the first channel of the sensing model (HS channel), it is meaningful to optimize the capacity of HS hybridized with AuNPs-DNA. Considering the amount of hybridized HS is equal to that of the participant DNA modified on AuNPs, it can be calculated with the as-built standard curve by measuring the fixed fluorescence intensity (Fig. S4A). As shown in Fig. S4B and S4C, the fluorescence intensity of cy3 varied along with the amount of HS and it reached a platform at 5187 arbitrary units (a.u.), suggesting that the hybridization effect of HS with the oligonucleotides on AuNPs was the maximum. Accordingly, the optimized concentration of HS to hybridize with AuNPs-DNA was 176 nM by calculation.

To achieve another channel (CDs-DNA channel) for sensing, the amount of CDs-DNA hybridized with AuNPs-DNA was optimized (Fig. 3A). As shown in Fig. 3B, the fluorescence intensity of excess CDs-DNA was recorded at 3470 arbitrary

units (a.u.). Hence, the concentration of excess CDs-DNA was 24.6 μg/mL by calculation with the as-built standard curve (Fig. S3C and S3D), and 70.8 μg/mL of CDs-DNA was proved as the optimized amount to hybridize with AuNPs-DNA. In view of the possible influence of incubation time on the hybridization procedures, various time (0 min, 2 min, 4 min, 6min, 8 min, 10 min, 12 min, 14 min, 16 min, 18 min, 20 min and 22 min) for the hybridization of CDs-DNA or HS with AuNPs-DNA have been also investigated. In Fig. S5A, the fluorescence of CDs-DNA constantly decreased until the reaction time reached 18 min, due to no more CDs-DNA left. Basically, the quenching mechanism between AuNPs and CDs was related with the fluorescence FRET. To be specific, the distance between the gold nanoparticles and carbon was less than 5 nm based on the current design of nucleotide sequence. Meanwhile, there emerged a spectral overlap between the absorption band of the AuNPs and the emission band of the CDs (Fig. S6A). Moreover, the lifetime of the CDs-DNA was 9.60 ns in the absence of AuNPs-DNA and varied to 8.13 ns in the prescence of AuNPs-DNA (Fig. S6B). Taken together, the fluorescence quenching mechanism here was reasonably considered as the FRET process. Thus, 18 min served as the optimal hybridization time between AuNPs-DNA and CDs-DNA. Analogously, the fluorescence increase of cy3 reached the maximum while the reaction time was more than 16 min, suggesting the hybridization between AuNPs-DNA and HS completely finished during 16 min (Fig. S5B). Taken the above data together, 18 min of incubation time was eventually identified for the following explorations.

On the whole, the dual-channel sensing model consisted of AuNPs-DNA, CDs-DNA and HS, and the sequences of CDs-DNA and HS completely match with that of AuNPs-DNA base to base. For constructing the dual-channel assay, we addressed whether this sensing model can be applied for detecting target RNA/DNA or not. Consequently, BRCA1 RNA and TK1 RNA were directly introduced into this model. Briefly, the addition of TK1 RNA brought a fantastic rising of the fluorescence intensity of cy3 (Fig. S7A). Simultaneously, a dramatic fluorescence decrease was observed while BRCA1 RNA added (Fig. S7B), indicating its satisfactory availability for detecting target nucleic acid. Furthermore, successfully analyzing the two different RNA illustrated this sensing model showed potential for assaying two nucleic acids during one single procedure.

To test the possible interference by BRCA1 RNA or TK1 RNA on each other during the assaying process, further experiments were designed in detail. As shown in Fig. S8A, the fluorescence at 435 nm obviously increased (λex=345 nm) with no fluorescence change at 565 nm while only BRCA1 RNA was introduced. At the same time, exciting the model at λ=535 nm dis not yield any fluorescence change at 565 nm, indicating that BRCA1 RNA yielded a fluorescence change for only CDs-DNA channel. Similarly, the subjection of only TK1 RNA to the sensing model resulted in the fluorescence decrease at 565 nm (λex=535 nm) rather than at 435 nm (λex=345 nm), implying that only the HS channel responded to the TK1 RNA (Fig. S8B). Finally, the two kinds of RNA were simultaneously added into the sensing model, and the fluorescence increasing at 435 nm (λex=345 nm) and decreasing at 565 nm

(λex=535 nm) occurred (Fig. S8C). This data confirmed that the excitation spectra of CDs and cy3 did not overlap, allowing to generate the selective fluorescence bands with no cross-impact. Taken together, this sensing model can be employed for separately assaying BRCA1 RNA or TK1 RNA without any interference by each other. For obtaining the optimized incubation time, various time (0 min, 2 min, 4 min, 6 min, 8 min, 10 min, 12 min, 14 min, 16 min, 18 min, 20 min, 22 min and 24 min) for reactions between BRCA1 RNA, TK1 RNA and the sensing model has been investigated. In Fig. S8A, the fluorescence increase of CDs-DNA reached the maximum once the reaction time was more than 20 min, suggesting the reactions of BRCA1 RNA with the model completed. Similarly, the fluorescence of cy3 constantly decreased while the reaction time was less than 20 min (Fig. S9B), suggesting the reactions between TK1 RNA and the model finished after 20 min. Therefore, 20 min of the incubation time was chosen for detecting the targets.

3.4 Detection of targets

Based on the designed sensing model, the standard cure of this method was established by various concentrations of BRCA1 RNA (4 nM, 10 nM, 20 nM, 30 nM, 50 nM, 70 nM, 80 nM, 100 nM and 120 nM) and TK1 RNA (8 nM, 10 nM, 20 nM, 30 nM, 40 nM, 50 nM, 70 nM, 100 nM and 120 nM). The results indicated that the fluorescence intensity of CDs-DNA increased proportionally with varied amounts of BRCA1 RNA added (Fig. 4A and 4B). Particularly, F/F_0 (where F_0 and F are the fluorescence intensities of CDs-DNA in the absence and in the presence of BRCA1 RNA respectively) increase versus the concentrations of BRCA1 RNA displayed a

linear range of 4-120 nM with its correlation coefficient of 0.991, and the detection limit was 1.5 nM at a signal-to-noise ratio of 3, suggesting its sensitivity and promising. Similarly, F_0/F (where F_0 and F are the fluorescence intensities of cy3 in the absence and in the presence of TK1 RNA respectively) decreased proportionally to the concentration of TK1 RNA in the range from 8 nM-120 nM, resulting in a typical dose-response curve together with its correlation coefficient of 0.992 (Fig. 4C and 4D), and the detection limit was 3.6 nM at a signal-to-noise ratio of 3.

Likewise, this dual-channel model exhibited excellent performance for DNA detections. Obviously, the fluorescence intensity of CDs-DNA increased with the addition of BRCA1 DNA. In particular, the fluorescence intensity increase versus the concentrations of BRCA1 DNA displayed a linear range of 4-120 nM together with its correlation coefficient of 0.985 (Fig. S10A and S10B), and the detection limit was 2.1 nM at a signal-to-noise ratio of 3. Meanwhile, the fluorescence intensity of cy3 decreased proportionally to the concentration of TK1 DNA in the range from 8 nM-120 nM, resulting in a typical dose-response curve with its correlation coefficient of 0.990 (Fig. S10C and S10D), and the detection limit was 4.5 nM at a signal-to-noise ratio of 3, which is similar to the RNA detection sensitivity achieved by the current sensing model. Hence, the data obtained here showed the promising practical applications of this strategy on directly detecting the target RNA and DNA.

In addition, the specificity of the sensing model designed here was investigated. As shown in Fig. S11A, the fluorescence intensity of CDs-DNA increased 107.4%, 67.0%, 22.6%, 3.8% and 2.4% in the presence of the targets including BRCA1 RNA,

single-base mismatched, three-base mismatched, five-base mismatched and random RNA with the same concentration (100 nM) respectively, indicating its satisfactory selectivity of the first sensing channel. In the same way, the fluorescence intensity of cy3 decreased 69.4%, 32.7%, 13.4%, 5.1% and 1.6% for analyzing the targets of TK1 RNA, single-base mismatched, three-base mismatched, five-base mismatched and random RNA respectively (Fig. S11B), showing its favorable selectivity of the second sensing channel. As the number of mismatched rose, the change of the fluorescence intensities respond less and less, demonstrating that the whole sensing model can obviously distinguish the full-matched and mismatched.

4. Conclusions

In summary, we hereby successfully established a fluorescent dual-channel model based on CDs-DNA, HS and AuNPs-DNA for assaying nucleic acids. For constructing the model, the fluorescence of CDs-DNA was quenched in the absence of targets. In a similar way, HS hybridized with AuNPs-DNA and resulted in recovering the fluorescence of cy3. Towards the purpose of detections, the targets could specifically bind with AuNPs-DNA and released the CDs-DNA in the presence of BRCA1 RNA/DNA. Meanwhile, HS could be released and induced to quench the fluorescence of cy3 in the presence of TK1 RNA/DNA. Significantly, this proposed strategy has established a dual-channel method, and achieved to assay two targets simultaneously. Besides, the selectivity and sensitivity for the targets of BRCA1 and TK1 respectively were basically acceptable, suggesting that this approach has provided a promising way for determining multiple nucleic acids. Moreover, the

current sensing strategy not only allows the analysis of BRCA1 RNA/DNA and TK1 RNA/DNA, but also builds up a model for assaying any possible nucleotides or aptamer-substrate complexes by appropriate programming.

Acknowledgements

We gratefully acknowledge financial support by Innovative Project on Designing and Screening Drug Candidates of Chongqing (cstc2015zdcy-ztzx120003), the Opening Research Project from the State Key Laboratory of Silkworm Genome Biology (sklsgb161718-6), Fundamental Research Funds for the Central Universities (XDJK2017D155).

References

[1] Jiang GX, Susha AS, Lutich AA, Stefani FD, Feldmann J, Rogach AL. Cascaded FRET in Conjugated Polymer/Quantum Dot/Dye-Labeled DNA Complexes for DNA Hybridization Detection. Acs Nano. 3 (2009) 4127-4131.

[2] Tay CY, Yuan L, Leong DT. Nature-Inspired DNA Nanosensor for Real-Time in Situ Detection of mRNA in Living Cells. Acs Nano. 9 (2015) 5609-5617.

[3] Su S, Fan JW, Xue B, Yuwen LH, Liu XF, Pan D, et al. DNA-Conjugated Quantum Dot Nanoprobe for High-Sensitivity Fluorescent Detection of DNA and micro-RNA. Acs Appl Mater Inter. 6 (2014) 1152-1157.

[4] Zhou WJ, Chen YL, Corn RM. Ultrasensitive Microarray Detection of Short RNA Sequences with Enzymatically Modified Nanoparticles and Surface Plasmon Resonance Imaging Measurements. Anal Chem. 83 (2011) 3897-3902.

[5] Shih CC, Chen PC, Lin GL, Wang CW, Chang HT. Optical and Electrochemical Applications of Silicon-Carbon Dots/Silicon Dioxide Nanocomposites. Acs Nano. 9 (2015) 312-319.

[6] Hu SL, Trinchi A, Atkin P, Cole I. Tunable Photoluminescence Across the Entire Visible Spectrum from Carbon Dots Excited by White Light. Angew Chem Int Edit. 54 (2015) 2970-2974.

[7] Nie H, Li MJ, Li QS, Liang SJ, Tan YY, Sheng L, et al. Carbon Dots with Continuously Tunable Full-Color Emission and Their Application in Ratiometric pH Sensing. Chem Mater. 26 (2014) 3104-3112.

[8] Huang H, Li CG, Zhu SJ, Wang HL, Chen CL, Wang ZR, et al. Histidine-Derived Nontoxic Nitrogen-Doped Carbon Dots for Sensing and Bioinnaging Applications. Langmuir. 30 (2014) 13542-13548.

[9] Fernando KAS, Sahu S, Liu YM, Lewis WK, Guliants EA, Jafariyan A, et al. Carbon Quantum Dots and Applications in Photocatalytic Energy Conversion. Acs Appl Mater Inter. 7 (2015) 8363-8376.

[10] Martindale BCM, Hutton GAM, Caputo CA, Reisner E. Solar Hydrogen Production Using Carbon Quantum Dots and a Molecular Nickel Catalyst. J Am Chem Soc. 137 (2015) 6018-6025.

[11] Wu WT, Zhan LY, Fan WY, Song JZ, Li XM, Li ZT, et al. Cu-N Dopants Boost Electron Transfer andPhotooxidation Reactions of Carbon Dots. Angew Chem Int Edit. 54 (2015) 6540-6544.

[12] Bao L, Zhang ZL, Tian ZQ, Zhang L, Liu C, Lin Y, et al. Electrochemical

Tuning of Luminescent Carbon Nanodots: From Preparation to Luminescence Mechanism. Adv Mater. 23 (2011) 5801-5809.

[13] Yu HJ, Zhao YF, Zhou C, Shang L, Peng Y, Cao YH, et al. Carbon quantum dots/TiO2 composites for efficient photocatalytic hydrogen evolution. J Mater Chem A. 2 (2014) 3344-3351.

[14] Wang X, Cao L, Yang ST, Lu FS, Meziani MJ, Tian LL, et al. Bandgap-Like Strong Fluorescence in Functionalized Carbon Nanoparticles. Angew Chem Int Edit. 49 (2010) 5310-5314.

[15] Hu C, Yu C, Li MY, Wang XN, Yang JY, Zhao ZB, et al. Chemically Tailoring Coal to Fluorescent Carbon Dots with Tuned Size and Their Capacity for Cu(II) Detection. Small. 10 (2014) 4926-4933.

[16] Deng JH, Lu QJ, Hou YX, Liu ML, Li HT, Zhang YY, et al. Nanosensor Composed of Nitrogen-Doped Carbon Dots and Gold Nanoparticles for Highly Selective Detection of Cysteine with Multiple Signals. Anal Chem. 87 (2015) 2195-2203.

[17] Zhang HJ, Chen YL, Liang MJ, Xu LF, Qi SD, Chen HL, et al. Solid-Phase Synthesis of Highly Fluorescent Nitrogen-Doped Carbon Dots for Sensitive and Selective Probing Ferric Ions in Living Cells. Anal Chem. 86 (2014) 9846-9852.

[18] Zhang LL, Han YJ, Zhu JB, Zhai YL, Dong SJ. Simple and Sensitive Fluorescent and Electrochemical Trinitrotoluene Sensors Based on Aqueous Carbon Dots. Anal Chem. 87 (2015) 2033-2036.

[19] Elghanian R, Storhoff JJ, Mucic RC, Letsinger RL, Mirkin CA. Selective

colorimetric detection of polynucleotides based on the distance-dependent optical properties of gold nanoparticles. Science. 277 (1997) 1078-1081.

[20] Song L, Guo Y, Roebuck D, Chen C, Yang M, Yang ZQ, et al. Terminal PEGylated DNA-Gold Nanoparticle Conjugates Offering High Resistance to Nuclease Degradation and Efficient Intracellular Delivery of DNA Binding Agents. Acs Appl Mater Inter. 7 (2015) 18707-18716.

[21] Rosi NL, Mirkin CA. Nanostructures in biodiagnostics. Chem Rev. 105 (2005) 1547-1562.

[22] Zhao Y, Cao L, Ouyang J, Wang M, Wang K, Xia XH. Reversible Plasmonic Probe Sensitive for pH in Micro/Nanospaces Based on i-Motif-Modulated Morpholino-Gold Nanoparticle Assembly. Anal Chem. 85 (2013) 1053-1057.

[23] Xiao ZY, Ji CW, Shi JJ, Pridgen EM, Frieder J, Wu J, et al. DNA Self-Assembly of Targeted Near-Infrared-Responsive Gold Nanoparticles for Cancer Thermo-Chemotherapy. Angew Chem Int Edit. 51 (2012) 11853-11857.

[24] Sedighi A, Li PCH, Pekcevik IC, Gates BD. A Proposed Mechanism of the Influence of Gold Nanoparticles on DNA Hybridization. Acs Nano. 8 (2014) 6765-6777.

[25] Peng HI, Strohsahl CM, Leach KE, Krauss TD, Miller BL. Label-Free DNA Detection on Nanostructured Ag Surfaces. Acs Nano. 3 (2009) 2265-2273.

[26] Shi JY, Chan CY, Pang YT, Ye WW, Tian F, Lyu J, et al. A fluorescence resonance energy transfer (FRET) biosensor based on graphene quantum dots (GQDs) and gold nanoparticles (AuNPs) for the detection of mecA gene sequence of

Staphylococcus aureus. Biosens Bioelectron. 67 (2015) 595-600.

[27] Raj JGJ, Quintanilla M, Mahmoud KA, Ng A, Vetrone F, Zourob M. Sensitive Detection of ssDNA Using an LRET-Based Upconverting Nanohybrid Material. Acs Appl Mater Inter. 7 (2015) 18257-18265.

[28] Yang YJ, Huang J, Yang XH, Quan K, Wang H, Ying L, et al. FRET Nanoflares for Intracellular mRNA Detection: Avoiding False Positive Signals and Minimizing Effects of System Fluctuations. J Am Chem Soc. 137 (2015) 8340-8343.

[29] Zu YB, Gao ZQ. Facile and Controllable Loading of Single-Stranded DNA on Gold Nanoparticles. Anal Chem. 81 (2009) 8523-8528.

[30] Demers LM, Mirkin CA, Mucic RC, Reynolds RA, Letsinger RL, Elghanian R, et al. A fluorescence-based method for determining the surface coverage and hybridization efficiency of thiol-capped oligonucleotides bound to gold thin films and nanoparticles. Anal Chem. 72 (2000) 5535-5541.

[31] Haiss W, Thanh NTK, Aveyard J, Fernig DG. Determination of size and concentration of gold nanoparticles from UV-Vis spectra. Anal Chem. 79 (2007) 4215-4221.

[32] Lee CH, Rajendran R, Jeong MS, Ko HY, Joo JY, Cho S, et al. Bioimaging of targeting cancers using aptamer-conjugated carbon nanodots. Chem Commun. 49 (2013) 6543-6545.

Figure captions

Scheme 1. Schematic illustration of the dual-channel sensing model for assaying multiple nucleotide sequences

Fig. 1. Characterization of AuNPs-DNA and CDs-DNA. (A) UV-vis absorption spectra of AuNPs and AuNPs-DNA, Inset: pho-tographs of AuNPs dissolved in water (a) and 0.3 M NaCl solution (b), AuNPs-DNA dissolved in 0.3 M NaCl solution (c) under day-light; (B) Fluorescence spectra of CDs (black) and CDs-DNA (red); (C) FTIR spectrum of CDs-DNA; (D) gel electrophoresis of DNA marker-A (lane 1), CDs alone (lane 2), DNA alone (lane 3), DNA (1 μM) with 0.02 mg/mL (lane 4), 0.04 mg/mL (lane 5), 0.08 mg/mL (lane 6), 0.12 mg/mL (lane 7) and 0.16 mg/mL (lane 8) CDs.

Fig. 2. Quantitation of thiol-oligonucleotides loaded on AuNPs. (A) Schematic illustration of identifying the amount of thiol-oligonucleotides modified on AuNPs; (B) Fluorescence spectra for different concentrations of HS hybridizing with displaced oligonu-cleotides; (C) Plot of the fluorescence intensity versus different concentrations of HS.

Fig. 3. Optimizing the amount of CDs-DNA hybridized with AuNPs-DNA. (A) Schematic illustration for identifying the amount of HS hybridized with AuNPs-DNA; (B) Fluorescence spectrum of excess CDs-DNA.

Fig. 4. (A) Fluorescence spectra of the sensing model in the presence of varied concentrations of BRCA1 RNA excited at λ=345 nm; (B) The linear relationship between F/F_0 and the concentrations of BRCA1 RNA; (C) Fluorescence spectra of this sensing model in the presence of varied concentrations of TK1 RNA excited at λ = 535 nm; (D) The linear relationship between F0/F and the concentrations of TK1 RNA.

Figures

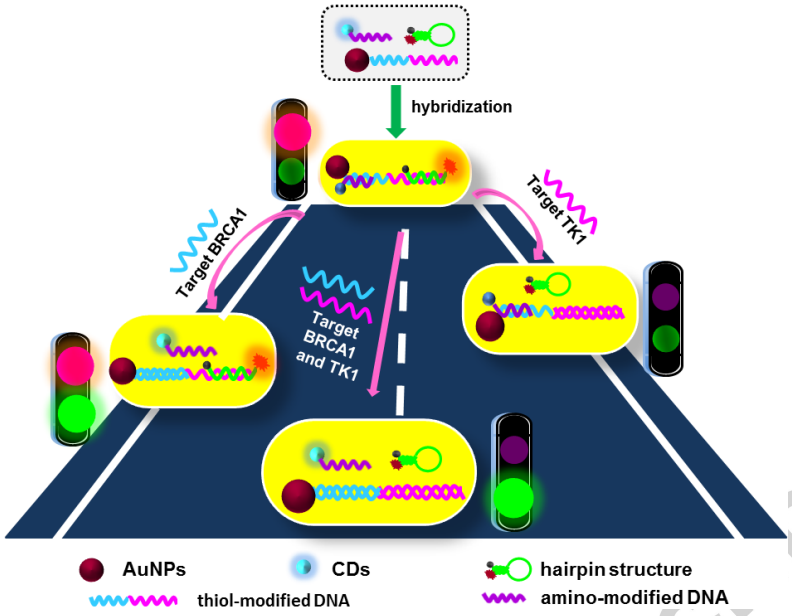

Scheme 1

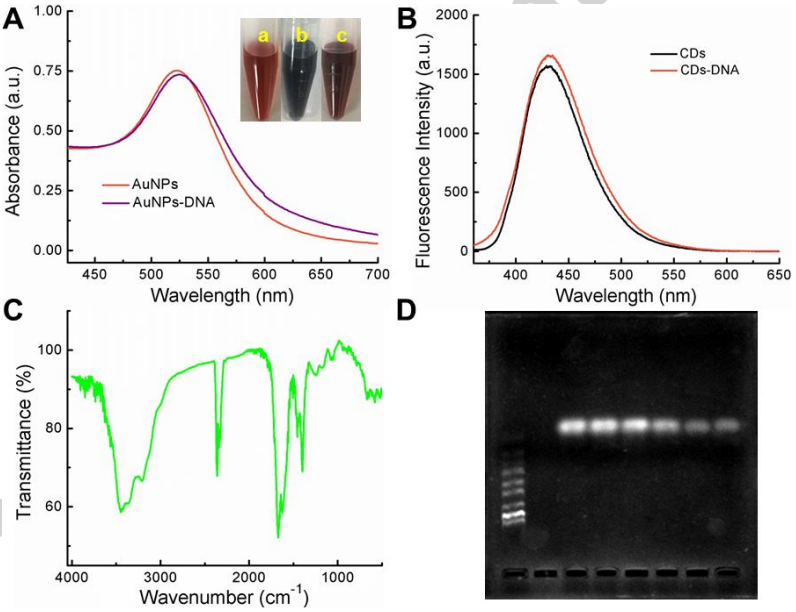

Fig. 1

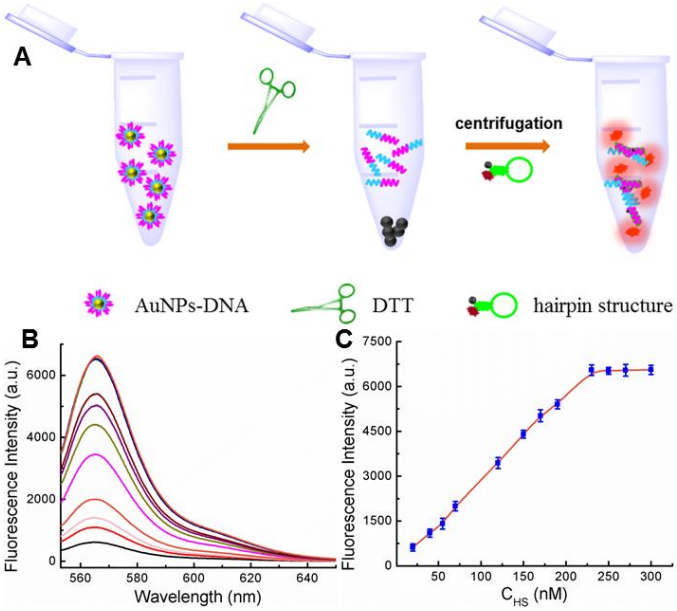
A
centrifugation
AuNPs-DNA
DTT
hairpin structure
B
Fluorescence Intensity (a.u.)
Wavelength (nm)
C
Fluorescence Intensity (a.u.)
C_HS (nM)

Fig. 2

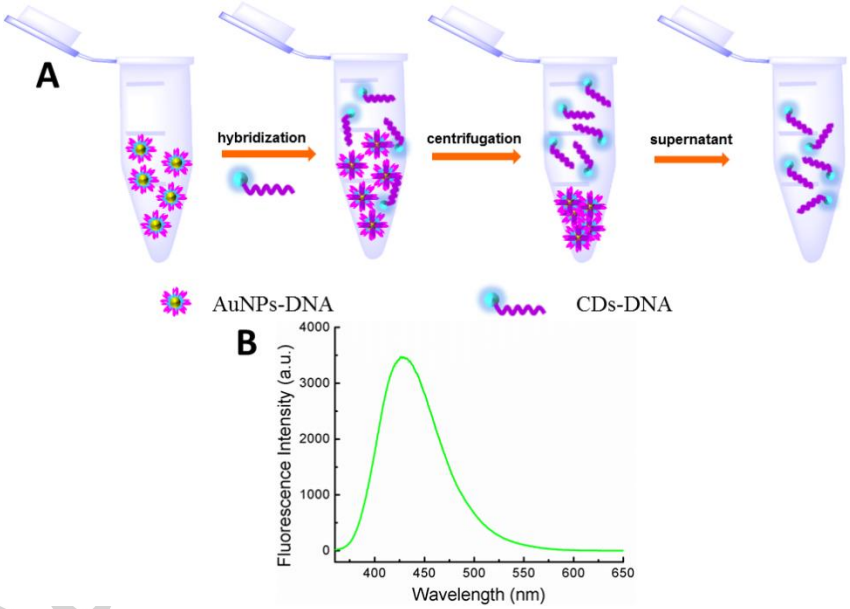
A
hybridization
centrifugation
supernatant
AuNPs-DNA
CDs-DNA
B
Fluorescence Intensity (a.u.)
Wavelength (nm)

Fig. 3

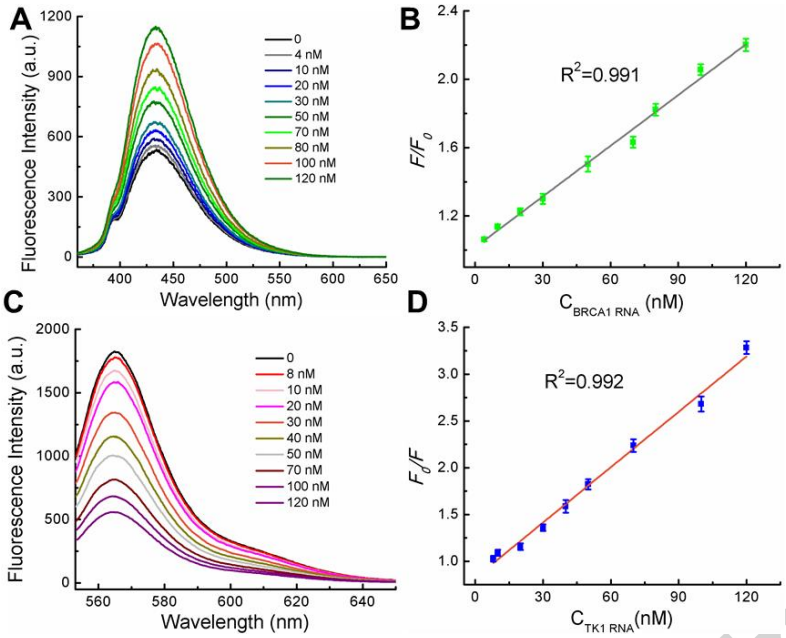

Fig. 4

Highlights

- Carbon dots (CDs) with blue fluorescence were synthesized and creatively modified.
- An innovative dual-channel biosensor on the basis of gold nanoparticles (AuNPs) was well-established
- This strategy has broadened avenues for assaying nucleic acid.
- This sensing model could assay any possible gene sequence or aptamer-substrate complexes by appropriately programming.